JOURNAL OF GEOPHYSICAL RESEARCH, VOL. 112, D10315, doi:10.1029/2006JD007857, 2007

Latitude-dependent long-term variations in polar mesospheric clouds from SBUV version 3 PMC data

Matthew T. DeLand,[1] Eric P. Shettle,[2] Gary E. Thomas,[3] and John J. Olivero[4]

Received 31 July 2006; revised 18 October 2006; accepted 15 January 2007; published 30 May 2007.

[1] Previous studies have suggested that there should be secular trends in polar mesospheric cloud (PMC) occurrence frequency and brightness on decadal timescales and that those trends would be strongest at the lowest latitudes of the PMC existence region. We have analyzed the 27-year PMC data set created from Solar Backscatter Ultraviolet (SBUV, SBUV/2) satellite instruments for long-term variations in albedo using three latitude bands (50°–64°, 64°–74°, 74°–82°). The improved version 3 data set includes revisions to the PMC detection algorithm to produce more consistent results in all measurement conditions. A detailed error analysis yields an approximate uncertainty of 1–2% for seasonally averaged 252-nm albedo values. Adjustments for local time variations in PMC brightness between different satellite data sets were derived to ensure accurate trend calculations. Multiple linear regression fits show that albedo variations are anticorrelated with solar activity in all latitude bands, with a stronger response at high latitudes. The albedo increase from solar maximum to solar minimum ranges from +2% at 50°–64°S to +17% at 74°–82°N. Secular trends in albedo are positive, with long-term changes over 27 years ranging from +12% to +20% depending on hemisphere and latitude. The derived long-term trend in PMC albedo at 50°–64° is smaller than that of higher latitudes. This result contradicts previous suggestions that PMC brightness changes might be most rapid at low latitudes. The albedo response to solar variations is larger in the Northern Hemisphere, while long-term trends are approximately the same in both hemispheres.

Citation: DeLand, M. T., E. P. Shettle, G. E. Thomas, and J. J. Olivero (2007), Latitude-dependent long-term variations in polar mesospheric clouds from SBUV version 3 PMC data, *J. Geophys. Res.*, *112*, D10315, doi:10.1029/2006JD007857.

1. Introduction

[2] Polar mesospheric clouds (PMC) are observed in the upper mesosphere at altitudes of 80–85 km during the summer season at high latitudes. There is now little doubt that the PMC particles are composed of water ice [e.g., *Hervig et al.*, 2001; *Eremenko et al.*, 2005] and thus form only in a limited altitude region where the mesospheric temperature falls below the frost point [*Lübken*, 2000]. *Donahue et al.* [1972] first demonstrated the continued presence of these clouds up to ~80°N using 2 years of satellite data and confirmed earlier observations [*Fogle*, 1965] that the phenomenon also exists in the Southern Hemisphere (SH). Satellite measurements of PMCs have been made regularly since late 1978 by overlapping SBUV and SBUV/2 instruments, providing a continuous database now extending over 27 years. *DeLand et al.* [2006] provided a recent review of the SBUV data, as well as other satellite PMC data sets collected during this period.

[3] The comprehensive geographic and temporal coverage of satellite PMC data enables quantitative studies of long-term variations. *Shettle et al.* [2002a] used data from three satellites with observations during periods of low solar activity to determine an increase in the number of bright Southern Hemisphere PMCs from 1983–1986 to 1993–1996. *Shettle et al.* [2002b] found an increase in bright PMCs in the Northern Hemisphere (NH) from 16 years of Stratospheric Aerosol and Gas Experiment (SAGE II) data. *DeLand et al.* [2003] analyzed PMC data from multiple Solar Backscatter Ultraviolet (SBUV, SBUV/2) satellite instruments covering 24 years and derived long-term variations. They found a significant anticorrelation between both occurrence frequency and brightness distribution with solar activity in both hemispheres using hemispherical averages of these data over full summer seasons. The PMC response was found to lag the solar activity variation by up to 1 year. Positive secular trends were also derived for both quantities in each hemisphere, with higher correlations for the brightness distribution results. *Thomas et al.* [2003] extended this analysis to the season-

[1] Science Systems and Applications, Inc. (SSAI), Greenbelt, Maryland, USA.
[2] Remote Sensing Division, Naval Research Laboratory, Washington, District of Columbia, USA.
[3] Laboratory for Atmospheric and Space Physics, University of Colorado, Boulder, Colorado, USA.
[4] Department of Physical Sciences, Embry-Riddle Aeronautical University, Daytona Beach, Florida, USA.

0148-0227/07/2006JD007857$09.00

ally averaged PMC albedos at 252 nm. They found statistically significant trends in both hemispheres, with the Southern Hemisphere albedo trend approximately twice as large as the Northern Hemisphere trend. *Shettle et al.* [2005] and *DeLand et al.* [2005] presented preliminary studies of latitude-dependent trends in SBUV PMC data.

[4] Long-term trends in PMC properties are most likely due to some combination of changes in mesospheric temperature and water vapor, since these factors control the existence of ice particles in the summer polar mesosphere. *Thomas et al.* [1989] proposed that the observed long-term increase in methane, which oxidizes to form water vapor in the upper stratosphere and mesosphere, could lead to increases in both PMC occurrence frequency and brightness. With regard to the possible latitude dependence of such changes, *Thomas* [1996] suggested that long-term increases in water vapor or decreases in mesospheric temperature may expand the latitude range of PMC occurrence toward the equator. *Shettle et al.* [2002a] proposed that "this region (60° to 70°S) near the outer edge of where PMCs are normally detected is particularly sensitive to changes."

[5] This paper presents analysis of trends in SBUV PMC brightness data as a function of latitude, extending the results discussed in *Thomas et al.* [2003]. In general, we will use the term "SBUV" to indicate both SBUV and SBUV/2 instruments. We use three broad latitude bands in each hemisphere (50°–64°, 64°–74°, 74°–82°) to get adequate statistics and comparable sampling between bands. We also calculate hemispherically averaged (50°–82°) results for comparison with our previous work. The occurrence frequency of PMCs is important as an overall indicator of PMC activity and for the determination of zonally averaged ice content [*Stevens et al.*, 2003]. However, in this work we concentrate on PMC albedo (also referred to as "brightness") because we feel that it is a more physically meaningful indicator of long-term variations, as discussed in the work of *Thomas et al.* [2003], and because it is the PMC property most readily measured by SBUV instruments. In addition, a proper treatment for local time (LT) variations in occurrence frequency (see section 4) requires further study. When adjusted SBUV frequency data are available, they will represent a more appropriate data set for comparison with long-term ground-based noctilucent cloud (NLC) observations.

[6] Section 2 describes some revisions to the PMC detection algorithm beyond those discussed in the work of *DeLand et al.* [2006]. Section 3 presents an uncertainty analysis for the PMC albedo values reported for SBUV measurements. SBUV instruments sample a range of local times at high latitudes, and the drifting orbits of some satellites (NOAA-9, NOAA-11, NOAA-14) produce significant changes in this range over time. Section 4 presents our derivation of a quantitative adjustment for local time variations in PMC albedo in order to perform the trend analysis. Section 5 describes the procedure used to merge the data from seven SBUV instruments for regression fitting. Section 6 presents the results of our multiple regression analysis in time and solar activity. Section 7 discusses the statistical and physical significance of the regression results. Section 8 presents the concluding remarks.

2. Algorithm Revisions

[7] The SBUV/2 instrument measure stratospheric profile and total column ozone using nadir view measurements of backscattered solar radiation in the middle ultraviolet (250–340 nm) wavelength region. *Thomas et al.* [1989] first developed an algorithm to identify PMCs in SBUV data using measurements of the five shortest wavelengths covering 252–292 nm. Polynomial fits are used to characterize the background albedo as a function of solar zenith angle (SZA) at each wavelength for a given day. This background is then subtracted from the data, and a series of tests are applied to the residual albedo values to separate PMCs from albedo changes due to stratospheric ozone fluctuations. *DeLand et al.* [2003] describes these tests in more detail. The residual backscattered albedo at 252 nm is used to represent the PMC brightness for statistical analysis, since it has the largest value relative to the background compared to other SBUV wavelengths used for PMC detection. Subsequently, *DeLand et al.* [2006] presented improvements to the data screening and background subtraction procedures that produced a version 2 (V2) data set. Those changes increased the residual albedo values calculated for each PMC detection, but did not revise the detection tests themselves. Careful examination of the V2 data products following the preparation of this work indicated that one of the detection tests was biased toward increased detection of PMCs in descending node data, corresponding to early morning local times in normal SBUV observations (Figure 1). This test quantified local albedo variability by calculating the standard deviation of background albedo values in each of 10 solar zenith angle (SZA) bins for each day of measurements. However, this method leads to larger standard deviation values at high SZA as the slope of the background increases. The binning procedure also led to inconsistent PMC detection tests within a single day, between different seasons and between different instruments.

[8] We therefore revised the algorithm so that the standard deviation threshold is now specified by a latitude-dependent quadratic fit, based on albedo data taken during the last 10 days of the Northern Hemisphere PMC season (defined as 30 days before summer solstice to 70 days after solstice). As discussed in the work of *DeLand et al.* [2003], we expect few, if any, valid PMC detections during the beginning and end of our nominal season. We found that increasing the derived threshold by a uniform factor of 1.3 reduced the PMC detection rate to ~0.5% at the ends of this season, consistent with our previous results and the detection cutoff observed by *Bailey et al.* [2005] with SNOE data. Further threshold increases were not useful because they removed many "faint" PMCs (clouds with brightness near the threshold), thus worsening the statistics for seasonal averages, while having little additional effect on the end-of-season detection rate. We also apply a screening test to reject any measurements with albedo values more than four standard deviations below the background fit, or more than four standard deviations above the background fit plus a nominal bright PMC

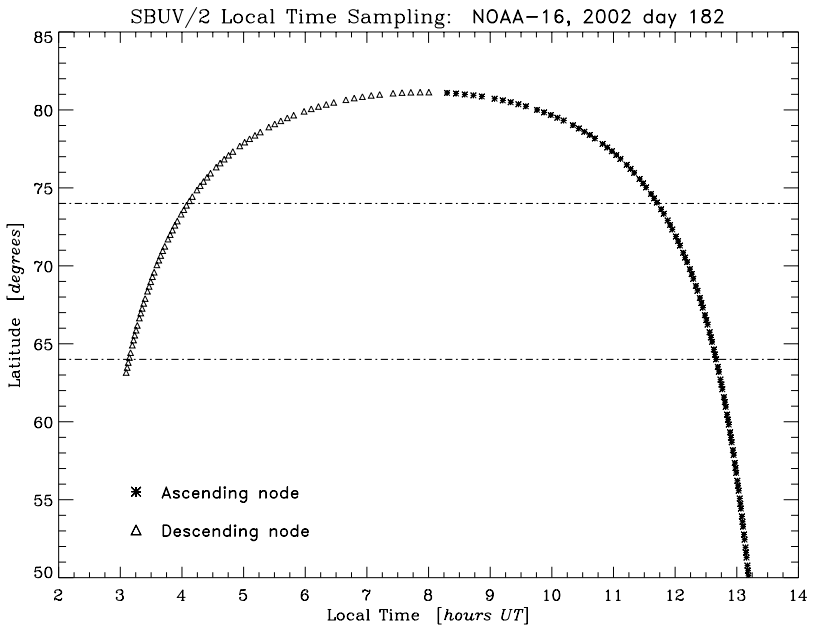

Figure 1. Variation of local time with latitude for one orbit of a typical SBUV instrument. Only every third sample is shown for clarity. The dot-dash lines separate the latitude regions (50°–64°, 64°–74°, 74°–82°) used in this study.

albedo value. This change is particularly important for NOAA-11 SBUV/2 data, where instrument grating drive errors [*DeLand et al.*, 2003, section 2.1.4] produce anomalous albedo values that would otherwise bias the background fit (most frequently toward lower albedo) and lead to false PMC detections. These revised SBUV data represent the version 3 (V3) PMC data product.

3. Albedo Uncertainty Analysis

[9] Determining an uncertainty value for the PMC albedos derived from SBUV PMC observations is a complex process. The following section presents a brief analysis of the key terms represented in the PMC albedo value. Table 1 lists numerical values of these terms for the three shortest wavelengths used in our analysis.

3.1. Radiometric Calibration

[10] Absolute calibration uncertainty values for SBUV radiance and irradiance measurements are discussed by *Hilsenrath et al.* [1995] and *Woods et al.* [1996], respectively. We neglect the NIST lamp uncertainty because the same set of lamps are typically used for both radiance and irradiance calibrations, and we assign an uncertainty of 2% to the bidirectional reflectance function of the radiance diffuser [*Janz et al.*, 1995]. The root-sum-square (RSS) of the remaining terms gives a value of 2.3% for the 250–300 nm wavelength range used here.

3.2. Background Fit

[11] Variations in the calculated background albedo include the accuracy of the fourth order polynomial fit (Figure 2b in the work of *DeLand et al.* [2003]) as well as geophysical fluctuations. We calculated the average PMC and background albedo values for narrow solar zenith angle intervals using randomly selected seasons. The derived relative uncertainty values of the background fit for 252-nm measurements are 22.6% at SZA = 40°, 19.3% at SZA = 60°, and 18.9% at SZA = 80°.

3.3. Out-of-Band Response

[12] The origin of this term is discussed in section 2.1.5 of the work by *DeLand et al.* [2003]. The correction values are empirically derived for each SBUV instrument. The magnitude of the out-of-band response (OOBR) correction for any measurement depends on wavelength, surface reflectivity, solar zenith angle, and total ozone amount. For a limited latitude range (i.e., small ΔSZA and constant total ozone) and time period (for example, 1 month), we can parameterize the derived correction as a linear function of surface reflectivity. The OOBR correction uncertainty was then estimated by applying this derived correction for a

Table 1. Albedo Uncertainty

Wavelength, nm	SZA	Radiometric Calibration, %	Background Fit, %	OOBR Correction, %	Measurement Noise, %	Long-Term, %	Total (RSS), %
252	40°	2.3	22.6	3	0.6	3.0	23.1
	80°	2.3	18.8	3	1.6	3.0	19.5
273	40°	2.3	32.1	10	0.1	3.0	33.8
	80°	2.3	20.3	10	0.3	3.0	22.9
283	40°	2.3	37.9	20	0.04	3.0	43.0
	80°	2.3	20.6	20	0.13	3.0	29.0

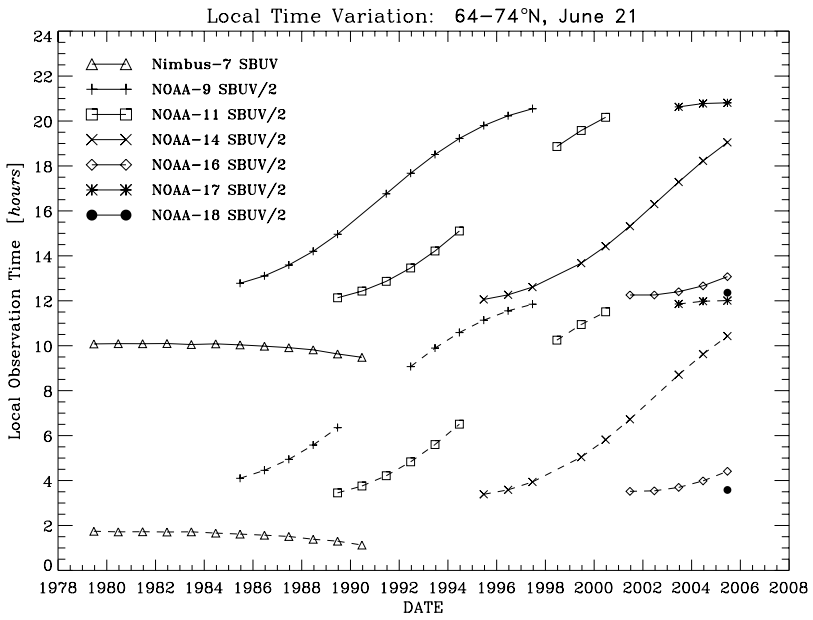

Figure 2. Variation of local time at 64°–74°N on June 21 for all SBUV instruments. Identifications for each instrument are given in the plot. Solid lines = ascending node data; dashed lines = descending node data.

specific instrument to observed data for selected months and calculating the residual slope. The relative uncertainty varies significantly as a function of reflectivity and SZA. We carry values of 3% at 252 nm, 10% at 273 nm, and 20% at 283 nm for further analysis.

3.4. Measurement Noise

[13] The SBUV/2 instrument measures incoming signals as the photomultiplier tube current, then digitizes these data and adds a nominal offset value to avoid counter underflow [*DeLand et al.*, 2001]. Measurement noise is evaluated by averaging samples taken on the night side with no incoming signal, so that only the electronic offset is observed. The relative uncertainty values listed in Table 1 decrease rapidly at longer wavelengths as the terrestrial albedo increases.

3.5. Instrument Degradation

[14] *Hilsenrath et al.* [1995] describes the derivation of SBUV/2 long-term albedo corrections in detail. Key instrument performance parameters such as solar diffuser reflectivity, wavelength calibration, and radiometric sensitivity are tracked using an onboard calibration system and dedicated measurements. In addition, "soft" calibration techniques using carefully chosen subsets of the science data provide information for instrument characterization [*Taylor et al.*, 2003]. By combining results from different methods, *DeLand et al.* [2004] determined a maximum calibration uncertainty of 3% over the lifetime of an SBUV/2 instrument.

3.6. Combined Uncertainty Estimate

[15] The final column of Table 1 lists the RSS albedo uncertainty for a single PMC at the three shortest SBUV wavelengths and two representative SZA values. Most of this uncertainty is composed of random variations. For the latitude band and seasonal averages reported in this paper, the albedo uncertainty will therefore be a factor of $N^{1/2}$ smaller than the standard deviation of the average value, where N is the number of PMCs observed. Typical full-season PMC totals are 100–400 at 50°–64° latitude, increasing to 500–2000 at 74°–82°. An estimated albedo uncertainty of 22% at 252 nm thus corresponds to a statistical uncertainty in the mean value of approximately 1.1–2.2% at 50°–64° latitude and 0.5–1.0% at 74°–82° for seasonally averaged results.

4. Local Time Variations

[16] Figure 1 shows the nominal SBUV orbit sampling for a Sun-synchronous orbit with an approximate equator-crossing time of 1400. During polar summer, sunlit measurements can be made on both the ascending and descending nodes of the orbit. As a result, any long-term PMC trend analysis using data above ~63° latitude will incorporate measurements from different local times, although continuous coverage is only possible near 80° latitude. This approach is complicated by the fact that the equator-crossing times of some SBUV instruments have drifted by many hours during their lifetimes, resulting in substantial long-term changes in local time coverage for each latitude band. This change in the mean local time of ascending and descending node measurements is shown in Figure 2 for each SBUV instrument for the 64°–74°N latitude band. Similar changes occur for the other latitude bands. We therefore need some method of characterizing local time effects in our measurements to accurately represent long-term PMC behavior. While the data points shown in Figure 2 do cover a wide range of local times, reasonably complete sampling only happens over many years. Variations in occurrence frequency and albedo due to solar activity and interannual variability would make it difficult to extract a diurnal signal directly from the observations. *Stevens et al.* [2004] examined local time variations in total ice mass at

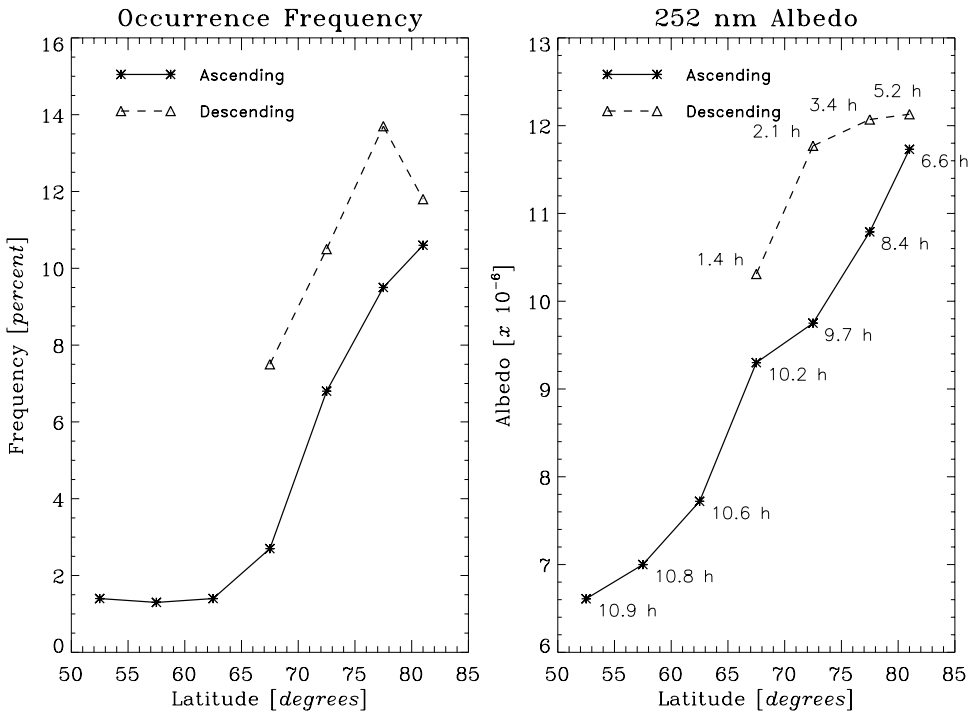

Figure 3. (a) Seasonal average PMC occurrence frequency for Nimbus-7 SBUV during the NH 1985 PMC season, calculated in 5° latitude bands (50°–55°, . . .75°–80°, 80°–82°). Asterisks = ascending node data; triangles = descending node data. (b) Seasonal average PMC albedo at 252 nm versus latitude for the Nimbus-7 SBUV NH 1985 season, using the same latitude bands as in Figure 3a. The average local time for each data point is also shown (same values as for Figure 3a).

70°N for NOAA-14 SBUV/2 data. We extend their work here to develop an adjustment for albedo data at all latitudes.

[17] Various groups have characterized PMC diurnal variations using lidar measurements. In particular, results obtained by *Fiedler et al.* [2005] at 69°N using the Arctic Lidar Observatory for Middle Atmosphere Research (ALOMAR) lidar system indicate that both NLC occurrence frequency and backscatter coefficient values are significantly enhanced during late evening and early morning hours, whereas results obtained from late morning through early evening hours are relatively constant. Examination of Figure 2 shows that SBUV ascending node measurements at 64–74°N are obtained between 9 and 21 hr local time (LT), while descending node measurements occur between 1 and 12 hr LT (approximately 9 hrs earlier). We might therefore anticipate that descending node occurrence frequency and albedo values will be larger than ascending node values at the same latitude. Since we typically consider zonally averaged satellite data (daily averages over 13–14 orbits per day), we do not expect an identical response to ground-based measurements taken at a single longitude. Figure 3a shows Nimbus-7 SBUV occurrence frequency values for the NH 1985 season, averaged in 5° bands between 50°–82° latitude. The descending node values (early morning hours) are higher than the ascending node values (early afternoon hours) whenever both measurements are available, with a maximum ratio of approximately 2.8 for the 65°–70° latitude band. Figure 3b shows average PMC albedo values at 252 nm for the same season and latitude bands. These data look very similar to the occurrence frequency results, although the magnitude of the descending/ascending ratio is much lower (maximum value = 1.21 at 70°–75°). The satellite results average together longitudinal variations in both phase and amplitude as well as short-term periodic variations [e.g., *Merkel et al.*, 2003], so it is expected that these ratios are smaller than the results at a fixed location such as the work of *Fiedler et al.* [2005].

[18] We calculated the ratio of descending node seasonally averaged albedo values at 64°–74°N to ascending node values in the same latitude band for all SBUV instruments. The albedo ratio values are plotted in Figure 4a as a function of descending node local time. The black squares show results binned in 1-hr local time bins for clarity. A relatively smooth variation is observed, with enhancements of approximately 1.1–1.3 at 2–5 hrs LT (relative to 10–13 hrs LT). Figure 4b shows albedo ratio results calculated using data at 64°–74°S. Some SH seasons have ascending node local times between 21 and 3 hr, and descending node local times between 5–11 hr. For these seasons, the albedo ratio was calculated as A_{asc} / A_{desc} and plotted in Figure 4b according to the ascending local time value. The early morning local time dependence is similar to the NH case. The SH late evening data also show enhanced albedo values.

[19] We characterize these albedo variations with linear fits for further use in trend analysis. The fit results that define the adjustment factor $R_{adjusted}(t_{local})$ are listed in Table 2. A constant adjustment factor was calculated for the SH late evening data because the available local time range is small. A separate analysis of NOAA-9 SBUV/2 data in narrow latitude bands showed no statistically sig-

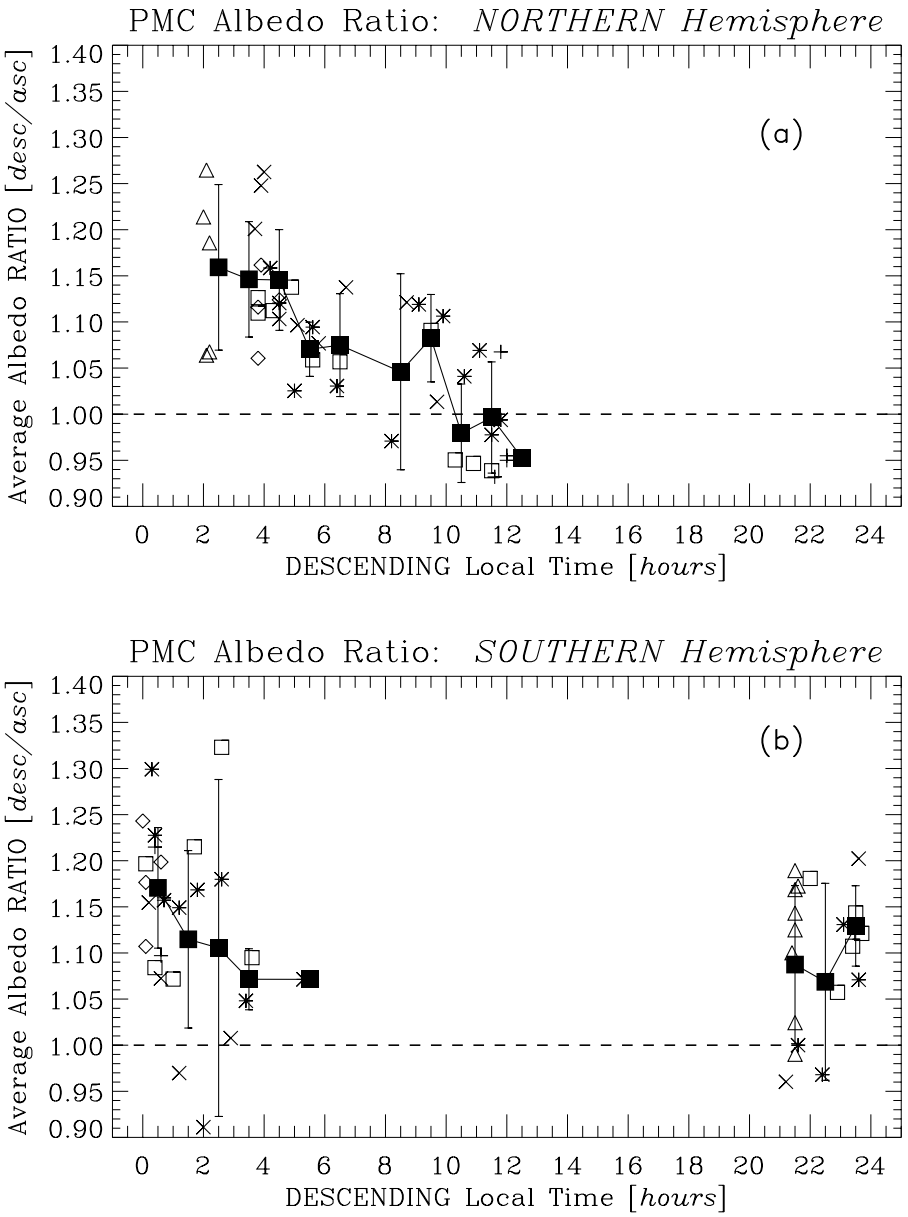

Figure 4. (a) Ratio of seasonally averaged 252-nm PMC albedo at 64°–74°N (descending/ascending data) for all SBUV instruments during 1979–2005, plotted as a function of descending node local time. Triangle = Nimbus-7, asterisk = NOAA-9, square = NOAA-11, cross = NOAA-14, diamond = NOAA-16, plus = NOAA-17, circle = NOAA-18. Black squares represent averages of all ratio values within each 1-hour local time bin. (b) Ratio of seasonally averaged 252-nm PMC albedo at 64°–74°S (descending/ascending data) for all SBUV instruments during 1979–2005. All symbol identifications are as in Figure 4a.

nificant latitude dependence in the albedo ratio values (in spite of the latitude dependence of the PMC residual albedo), so we apply these adjustments to all data samples with appropriate local time values. The variability of the albedo ratio data about these fits gives an uncertainty of approximately ±0.06 for the NH adjustment factor and ±0.10 for the SH adjustment factor. This adjustment is only applied to descending node data, which represent roughly half of the SBUV PMC detections depending on latitude (fewest at 50–64°). We therefore scale these results by a factor of two to determine a seasonal average albedo uncertainty due to our local time adjustment of ∼3% for NH data and ∼5% for SH data. We emphasize that this process is designed to remove sampling-related artifacts that could corrupt trend analysis and does not represent the correction of an error in the satellite PMC data.

Table 2. Albedo Adjustment Factors

	Factor	Time, hr
	$A_{adjusted} = A_{observed}/R_{adjusted}$	
Northern Hemisphere	$R_{adjusted} = 1.209 - 0.0187 \times t_{local}$	$t = 0–11.5$
Southern Hemisphere	$R_{adjusted} = 1.168 - 0.0224 \times t_{local}$	$t = 0–8$
	$R_{adjusted} = 1.098$	$t = 20–24$

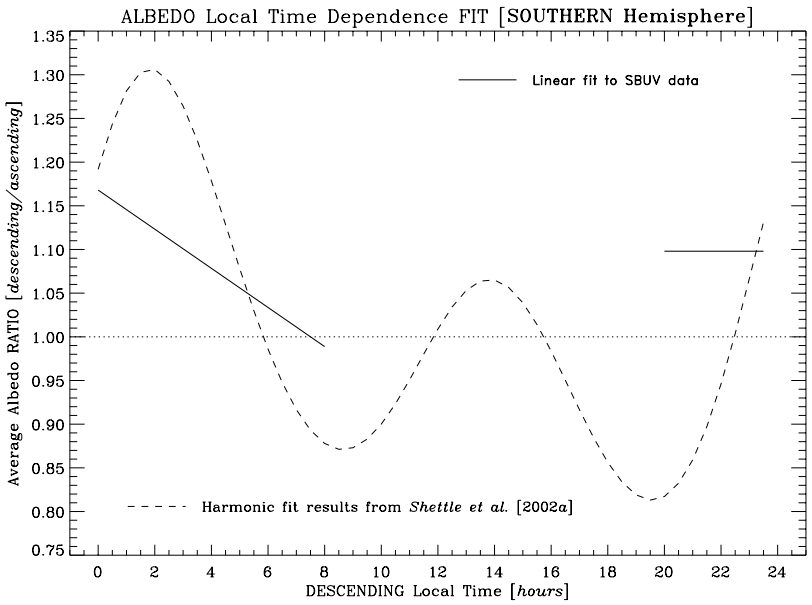

Figure 5. Comparison of PMC albedo diurnal variations from satellite instruments. Solid line = linear regression fit to SBUV 64°–74°S albedo ratio data shown in Figure 4b. Dot-dash line = harmonic fit to WINDII diurnal variations from *Shettle et al.* [2002a], plotted as $A(t_{\text{descending}})/A(t_{\text{ascending}})$, where $t_{\text{asc}} = t_{\text{desc}} - 8$ hours. See text for more details.

[20] The comparison of "point source" lidar NLC results for diurnal variations [e.g., *Chu et al.*, 2001; *Thayer et al.*, 2003; *Fiedler et al.*, 2005] with our zonally averaged PMC results is potentially complex and beyond the scope of this paper. *Shettle et al.* [2002a] derived a harmonic fit for local time variations in the zonally averaged excess extinction ratio observed by the Wind Imaging Interferometer (WINDII) instrument on the Upper Atmospheric Research Satellite (UARS). Their function, converted to the descending/ascending ratio format used in this paper, is shown in Figure 5 compared to the Southern Hemisphere local time variation derived from SBUV PMC data. The correspondence is not exact, but is still consistent with both early morning and late evening PMC brightness enhancements. This agreement is notable considering that the WINDII data only covered the period 5.5–20.5 hrs LT (so the harmonic fit is well constrained over that time period), although the harmonic fit was extended to cover the full day. The SBUV measurements do not cover enough local times to evaluate all parts of the result by *Shettle et al.* [2002a].

5. Merging of Data Sets

[21] The PMC data set analyzed in this paper includes data from seven SBUV and SBUV/2 instruments over a 27-year period from November 1978 through February 2006. In order to derive long-term variations in PMC albedo from the combined data, it is necessary to construct a single averaged value for seasons when more than one SBUV/2 instrument is operating. An important part of this process is the identification of problems or anomalies that would influence such an analysis.

5.1. Temporal Coverage During Season

[22] In some cases, complete temporal coverage is not available for a season because of instrument problems. Since the typical PMC albedo varies during the season [e.g., *Bailey et al.*, 2005], long data gaps can bias the seasonally averaged albedo relative to a complete season result. We have redundant measurements from other SBUV instruments during almost every season when such gaps are

Table 3. PMC Seasons Excluded From Trend Analysis

Satellite	Season	Reason for Exclusion
Nimbus-7 SBUV	NH 1987	Nonsync noise problems
	NH 1988	Nonsync noise problems
	NH 1989	Nonsync noise problems
	NH 1990	Nonsync noise problems
	SH 1987–1988	Nonsync noise problems
	SH 1988–1989	Nonsync noise problems
	SH 1989–1990	Nonsync noise problems
NOAA-9 SBUV/2	NH 1990	Terminator crossing effects
	NH 1993	Missing data (days 213–242)
	NH 1995	Missing data (days 215–242)
	NH 1996	Missing data (days 143–169)
	NH 1997	Limited data coverage (days 196–242)
	SH 1990–1991	Terminator crossing effects
	SH 1994–1995	Missing data (1995 days 44–54)
	SH 1997–1998	Limited data coverage (4 orbits per day)
NOAA-11 SBUV/2	NH 1995	No data available
	NH 1996	No data available
	NH 1997	Missing data (days 142–195)
	SH 1988–1989	Missing data (days 325–335)
	SH 1995–1996	No data available
	SH 1996–1997	No data available
NOAA-14 SBUV/2	NH 1995	Missing data (days 223–236)
	NH 1998	Missing data (days 171–181)
	NH 2002	Terminator crossing effects
	SH 2001–2002	Terminator crossing effects
	SH 2002–2003	Terminator crossing effects
NOAA-16 SBUV/2	NH 2004	Excessive instrument noise
	SH 2003–2004	Excessive instrument noise
NOAA-17 SBUV/2	NH 2002	Missing data (days 142–191)

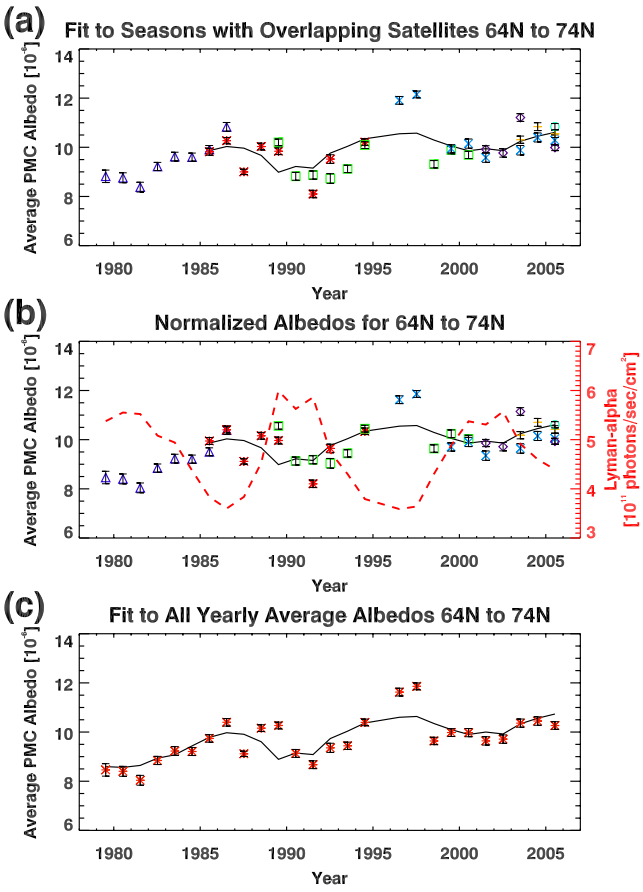

Figure 6. (a) Seasonally averaged PMC albedo values at 252 nm from SBUV and SBUV/2 instruments at 64°-74°N from 1979 to 2005. Triangle = Nimbus-7, asterisk = NOAA-9, square = NOAA-11, cross = NOAA-14, diamond = NOAA-16, plus = NOAA-17, circle = NOAA-18. $\pm 1\sigma$ standard error bars are shown. The solid line represents a multiple regression fit to data between 1985 and 2005 used only for normalization (see text). (b) PMC albedo for each instrument after normalization of interinstrument differences. The dashed line shows the average solar Lyman alpha flux for each season as discussed in section 6, scaled to fit on the same plot. The solid line is the same fit as in Figure 6a. (c) Combined average albedo values for all seasons at 64°–74°N. Solid line shows the multiple regression fit to the full data set from 1979 to 2005 using equation (1).

observed, so we have not attempted to replace the missing data based on any type of functional fit to the daily albedo values. We therefore eliminated these partial seasons to avoid the possibility of such biases affecting the results. Table 3 lists all seasons with data gaps greater than 10 days that have been excluded from the trend calculations. This conservative approach leaves us with no PMC data only for the Northern Hemisphere 1995 season. Figure 6a shows the remaining 64°–74°N albedo values after excluding the appropriate seasons.

5.2. Nimbus-7 SBUV Instrument Noise

[23] The Nimbus-7 SBUV instrument developed a problem with chopper wheel synchronization in February 1987 [*Gleason and McPeters*, 1995], leading to increased noise in the observed albedo values. This effect produces an apparent large increase (a factor of 3–4) in the number of faint PMCs detected by our algorithm at 50°–64° latitude. At higher latitudes, the seasonal average frequency looks more similar to previous years, but the average albedo may be reduced due to the addition of many faint PMCs caused by noise fluctuations. Because we do not have a method to quantify the possible albedo change caused by these "nonsync" data, we have excluded Nimbus-7 data for 1987–1990 from the trend analysis.

5.3. Albedo Threshold

[24] Examination of albedo data at 50°–64° latitude showed that some low seasonal averages for NOAA-11 SBUV/2 were caused by a high fraction (up to 35–40%) of PMC detections with 252-nm residual albedo values less than 5×10^{-6}. Such low values were seen in less than 1% of detections at these latitudes for all other SBUV instruments and essentially never at higher latitudes. Since the NOAA-11 SBUV/2 instrument also suffered from grating drive problems that increased instrument noise during a part of its lifetime, we decided to require a minimum value of $A_{252\ \mathrm{nm}} = 5 \times 10^{-6}$ for seasonal average calculations. This change brought the NOAA-11 results in line with other concurrent measurements. We reiterate that implementing this threshold did not affect the seasonal average results calculated for any other instrument or latitude band.

5.4. Data Set Normalization and Combination

[25] *Christy and Norris* [2004] discussed the challenges of combining many overlapping satellite data sets over a period of decades for tropospheric temperature data. They distinguish between a "backbone" technique in which a single best path is defined to connect successive data sets and a "consensus" approach that defines a statistically best path using all available overlap periods. After testing various methods, such as simple averaging within each season, we chose the following implementation of the consensus approach. First, a multiple regression fit in time and solar activity (described further in section 6) is applied to all data in each latitude band for the period with multiple satellites (1985–2005). This fit, shown as the solid line in Figure 6a, provides the reference level for normalizing each instrument's data to a common basis. Next, we take the ratio between each seasonal average albedo value and the reference fit. Most normalization values for individual seasons fall between 0.97–1.03, with only a few values exceeding ±5% of the seasonally averaged albedo at low latitudes. We note that the local time adjustment presented in section 4 reduces the difference of the normalization factors from 1.0 by approximately one-third compared to results derived using unadjusted data. We then compute an average normalization ratio for each SBUV instrument and adjust all seasons by this factor. Figure 6b shows an example of the normalized data for 64°–74°N. The changes from Figure 6a are small on this plot scale. The normalization process minimizes the ensemble of albedo differences for each instrument relative to the reference fit, so that interinstrument differences in individual seasons may either increase or decrease slightly after normalization. Figure 6c shows the combined normalized albedo data for each season at 64°–

Table 4. The 252 nm PMC Albedo Trend Fits[a]

Latitude	Solar Coefficient	Trend Coefficient	Constant	Lag (years)	Solar Cycle	Long-term Change	95% Confidence
50–64°N	−0.216 (±0.040)	0.037 (±0.005)	8.070	0.5	7.2%	12.6%	4.5%
64–74°N	−0.562 (±0.040)	0.063 (±0.004)	11.574	0.5	14.7%	16.9%	8.7%
74–82°N	−0.759 (±0.025)	0.067 (±0.003)	14.312	0.5	16.7%	15.1%	8.4%
50–82°N	−0.706 (±0.022)	0.067 (±0.002)	13.174	0.5	16.9%	16.4%	9.1%
50–64°S	−0.057 (±0.058)	0.035 (±0.006)	7.072	2.0	2.0%	12.7%	6.7%
64–74°S	−0.362 (±0.046)	0.066 (±0.005)	9.811	1.0	10.3%	19.9%	7.5%
74–82°S	−0.519 (±0.027)	0.050 (±0.003)	12.918	1.0	11.9%	12.2%	8.3%
50–82°S	−0.406 (±0.026)	0.058 (±0.003)	11.615	1.0	9.9%	15.2%	8.0%

[a]Solar coefficient (A_{solar}) = [(photons $cm^{-2}/sec^{-1})^{-1}$]. Lyman alpha flux values divided by 10^{11} for fit calculations; Trend coefficient (B_{trend}) = [albedo/year]. PMC albedo values divided by 10^{-6} for fit calculations; "Solar Cycle" = Calculated albedo increase from solar minimum to solar maximum (minimum flux = 3.5×10^{11} photons cm^{-2} sec^{-1}, maximum flux = 6.0×10^{11} photons cm^{-2}/sec^{-1}); "Long-Term Change" = Calculated albedo increase due to the linear trend over 27 years in the Northern Hemisphere and 28 years in the Southern Hemisphere; "95% Confidence" = Minimum long-term albedo change detectable at the 95% confidence level using equation (2).

74°N and a least squares fit to these data calculated using equation (1) as presented in section 6. We discuss this fit in more detail in the next section. For a regression fit analysis such as this one that includes multiple overlapping data sets, the data farthest from the midpoint of the time range have the most influence on the linear trend because they have the largest statistical lever arm. Thus the scaling factors for data sets such as Nimbus-7 SBUV (early) and NOAA-17 SBUV/2 (recent) are particularly important in determining the overall trend at each latitude. While other methods of combining data sets can produce a different latitude dependence for the linear trend, all methods that we tested yielded positive secular trends.

[26] SBUV-type instruments detect PMCs against a background that includes albedo fluctuations primarily because of stratospheric ozone variations. As a result, we identify only the brightest PMCs within the overall distribution. Measurements from limb-viewing instruments (for example, Student Nitric Oxide Explorer (SNOE) [*Bailey et al.*, 2005]) indicate that PMC occurrence frequencies reach ~80–90% at 80° latitude during the core of the season, much higher than any values observed by SBUV instruments. Thus the SBUV background fit at high latitudes includes some PMCs whose brightness is below our detection threshold, and the absolute value of the observed PMC albedo is slightly smaller than we would calculate if ideal "clear sky" background data containing no PMCs were available. Although we do not have a precise estimate of this effect on our albedo values, we note that our detection algorithm is applied consistently to all measurements over 27 years of data, so that any such contribution is present in each season. Thus any bias in high-latitude PMC albedo values should not affect the determination of time-dependent variations in PMC properties.

6. Regression Fits and Results

[27] The normalized and averaged PMC albedo data are fit with a multiple linear regression equation as described by *DeLand et al.* [2003] and *Thomas et al.* [2003] and shown in equation (1). Solar activity is represented by Lyman alpha flux values derived from the work of *Woods et al.* [2000] averaged over the nominal 100-day PMC season defined in section 2. Lyman alpha flux values from 2002 to the present are taken from the Thermosphere Ionosphere Mesosphere Energetics and Dynamics Solar EUV Experiment data [*Woods et al.*, 2005]. The Lyman alpha data were obtained from the Laboratory for Atmospheric and Space Physics (LASP) Interactive Solar Irradiance Datacenter (http://lasp.colorado.edu/lisird). The seasonally averaged Lyman alpha flux time series for Northern Hemisphere data is also shown in Figure 6b for illustration.

$$Y = A_{\mathrm{solar}} F_{Ly-\alpha}(t_{\mathrm{season}} - t_{\mathrm{lag}}) + B_{\mathrm{trend}}(t_{\mathrm{season}} - 1979) + C \quad (1)$$

[28] Regression fits were calculated using phase lag values t_{lag} (positive = PMC data trailing solar data) ranging from 0.0 to +3.0 years in 0.5-year increments, corresponding to the observed Northern Hemisphere and Southern Hemisphere PMC seasons. While smaller phase lag steps could be used, we found in the work of *DeLand et al.* [2003] that the statistically "best" value was not sharply defined. This is consistent with the results obtained by *Hervig and Siskind* [2006], who determined "best" phase lag ranges of 0.0–2.0 years for regression fits between solar Lyman alpha flux and PMC extinction, 80-km water vapor, and mesopause temperature as measured by the Halogen Occultation Experiment (HALOE) instrument. The fit results presented here correspond to the lag value that gives the highest multiple regression correlation coefficient and lowest χ^2 value for each latitude band and are summarized in Table 4. The uncertainty in the phase lag is about ±1.0 years, so the difference in phase lag value between +0.5 years for Northern Hemisphere cases and +1.0 years for most Southern Hemisphere cases should not be considered significant. The larger phase lag value of +2.0 years at 50°–64°S has little importance because the solar coefficient is small and has a comparatively large uncertainty. We cannot rule out the possibility of zero phase lag on statistical grounds, but we note that the persistent positive phase lag is consistent with the results of the work by *Hervig and Siskind* [2006], as well as multiple sets of ground-based measurements of NLC [*Thomas and Olivero*, 2001]. An example of the calculated long-term variation of PMC albedo at 64°–74°N is shown in Figure 6c together with the normalized and merged seasonal average albedo values.

[29] At this time, we have not tried to use more complex functions, such as multisegment linear or quadratic fits, to represent the time-dependent variation in PMC albedo. Such functions may in fact be more accurate descriptions of the long-term behavior, and they have been suggested based on

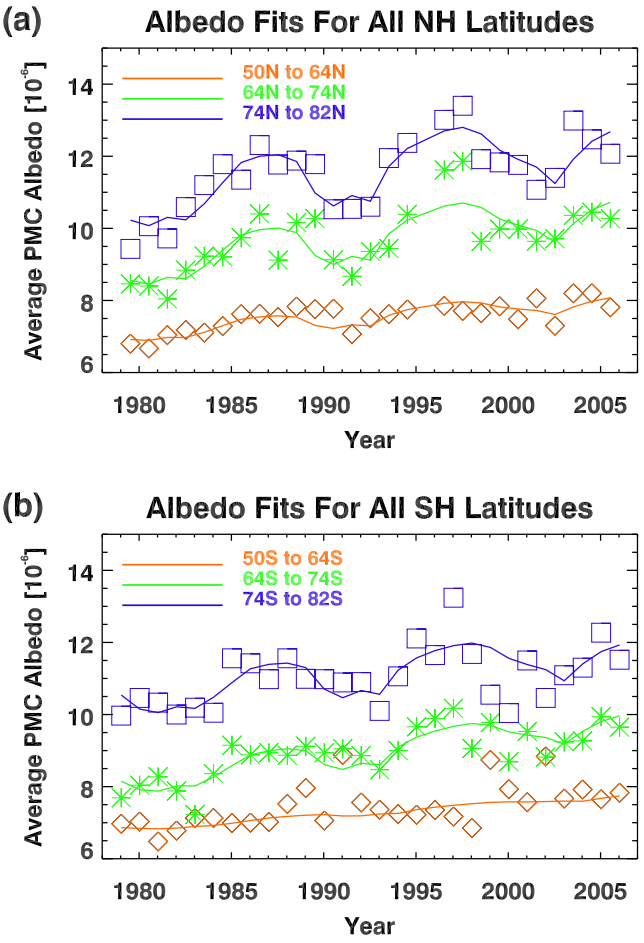

Figure 7. (a) PMC seasonal average albedo values and multiple regression fits for three Northern Hemisphere latitude bands for the full 1979–2005 period using the fit parameters listed in Table 4. Diamond = 50°–64°N, asterisk = 64°–74°N, square = 74°–82°N. (b) PMC seasonal average albedo values and multiple regression fits for three Southern Hemisphere latitude bands for the full 1979–2005 period using the fit parameters listed in Table 4. All symbol identifications are as in Figure 7a, but for SH latitudes.

observations of mesospheric water vapor changes [*von Zahn et al.*, 2004]. However, we prefer to have a firmer basis for moving beyond a linear time dependence, since the physical mechanism connecting mesospheric variability and PMC response is not yet established. We plan a further investigation of this issue.

[30] Figure 7a shows the individual averaged PMC albedo values for each season in the three Northern Hemisphere latitude bands and the calculated albedo variations for each latitude band. The fit coefficients for each latitude band and the hemispheric averages for 50°–82° are listed in Table 4, along with the statistical uncertainty for each coefficient. All of the fit terms are highly statistically significant, with the exception of the solar response at 50°–64°S. The calculated PMC albedo values are latitude dependent, with the average albedo increasing by slightly over 50% from 50°–64°N to 74°–82°N. The solar response and trend coefficients listed in Table 4 increase significantly from 50°–64°N to 64°–74°N then show smaller increases at 74°–82°N. If the regression coefficients are normalized to remove the effect of the albedo increase with latitude, the solar coefficient at 74°–82°N is slightly smaller than the value at 64°–74°N. However, the difference is within the ±1 σ range of each coefficient.

[31] This result differs from earlier presentations of SBUV/2 PMC albedo data in which the derived albedo trends at 50°–64° latitude were considerably larger than at higher latitudes. *Shettle et al.* [2005] imposed a conservative minimum brightness threshold of $A_{PMC} > 7 \times 10^{-6}$, as recommended by *Thomas et al.* [2003] based on hemispheric averages. Applying this approach to latitude dependence studies led to marginal statistics in the lowest latitude band, where only a small fraction of PMC detections exceeded this albedo threshold. The revised detection procedure discussed in section 2 provides a more robust and equitable treatment of fainter PMCs at all latitudes, so we feel comfortable in removing this threshold. As noted previously, the method of joining multiple data sets can affect the trend derived from the combined data and the relationship between different ensembles (for example, latitude bands). Specifically, *Thomas et al.* [2003] and *DeLand et al.* [2005] used simple averaging for seasons with overlap, which magnifies the impact of early seasons such as Nimbus-7 SBUV 1979–1984 where later seasons from that instrument show an offset with overlapping NOAA-9 data. The largest interinstrument offsets (especially in the V2 data) are found at the lowest latitude band, so the latitude dependence derived by *DeLand et al.* [2005] gave the largest trend there.

[32] The calculated Southern Hemisphere albedo results are shown in Figure 7b. The absolute albedo values are smaller than the corresponding Northern Hemisphere values in each latitude band, but show a comparable increase from lowest to highest (slightly less than 50%). The latitude dependence of the fit coefficients is similar to the NH result, with the largest increase from 50°–64°S to 64°–74°S. The normalized trend coefficient at 64°–74°S is somewhat larger than the normalized 74°–82°S coefficient because the Nimbus-7 SBUV data at 74°–82°S shifted upward following the normalization procedure, thus reducing the overall trend. Comparison of Northern Hemisphere and Southern Hemisphere fit coefficients shows that the derived solar response is consistently larger in the Northern Hemisphere at all latitudes, while the trend results are essentially the same in both hemispheres. This conclusion differs from previous results shown in the works of *DeLand et al.* [2003] and *Thomas et al.* [2003], where the Southern Hemisphere trend was approximately twice as large as the Northern Hemisphere trend. However, the hemispheric average trend results presented in the work of *DeLand et al.* [2006], based on V2 data and the interinstrument normalization method described in section 5, were more nearly equal (NH coefficient = 6.4×10^{-2} year^{-1}; SH coefficient = 7.8×10^{-2} year^{-1}, where albedo values have been divided by 10^{-6} for trend calculations). The 50°–82°N and 50°–82°S trend values listed in Table 4 are also similar to these results, although the Northern Hemisphere trend is now slightly larger than the Southern Hemisphere trend. Figure 8 shows the calculated full hemisphere albedo fits together with the results from the individual latitude

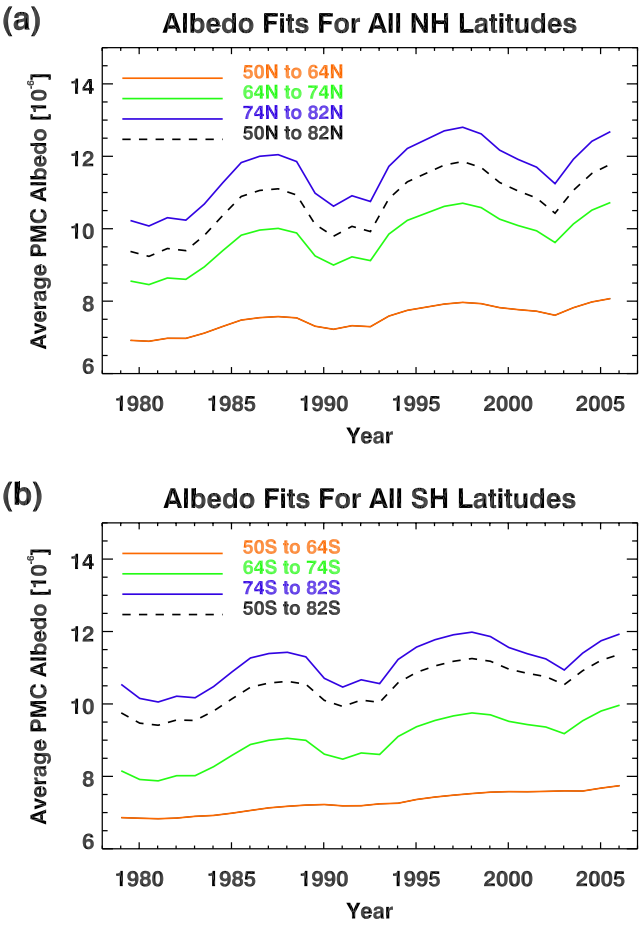

Figure 8. (a) PMC albedo multiple regression fits for Northern Hemisphere latitude bands 50°–64°, 64°–74°, 74°–82°, and 50°–82°. (b) PMC albedo multiple regression fits for Southern Hemisphere latitude bands 50°–64°, 64°–74°, 74°–82°, and 50°–82°.

bands. This illustrates our previous statement that the numerical results obtained from a composite data set are sensitive to the method used to create that data set.

[33] We have also calculated the predicted solar cycle and long-term PMC albedo variations for each latitude band, using the coefficients listed in Table 4. Solar cycle variations from minimum to maximum generally range between 7% and 17%, although the calculated solar variation at 50°–64°S is significantly smaller. The long-term albedo change over 27 years calculated using the regression fit results ranges in magnitude from approximately +12–13% at 50°–64°N, 50°–64°S, and 74°–82°S to +20% for 64°–74°S.

7. Discussion

[34] *Weatherhead et al.* [1998] discussed the issues involved in detecting a long-term trend in environmental data. They use deseasonalized data, for example, stratospheric temperature or total ozone, to evaluate the length of time required for trend detection. In our analysis of long-term PMC albedo variations, the Lyman alpha flux term represents this quasiperiodic variation. Note that this choice does not require a specific physical connection between solar activity and PMC properties. We then rearrange equation (3) of the work by *Weatherhead et al.* [1998] to estimate the magnitude of the PMC albedo trend that can be detected (at the 95% confidence level) using 27 years of data.

$$\omega_0 \approx \frac{3.3(\sigma_N + \sigma_{LT})}{n^{*3/2}}\sqrt{\frac{1+\varphi}{1-\varphi}} \quad (2)$$

ω_0 = trend magnitude
σ_N = variance of noise (seasonal average albedo relative to multiple regression fit)
σ_{LT} = estimated local time adjustment uncertainty
φ = autocorrelation
n^* = number of years of data

[35] For the example of PMC albedo data at 64°–74°N, we find that $\sigma_N = 0.51 \times 10^{-6}$, $\sigma_{LT} = 0.29 \times 10^{-6}$, and $\varphi = 0.44$. Equation (2) therefore says that we can detect a trend of 8.7% over 27 years in this latitude region with statistical confidence. The corresponding significance values for each latitude band are listed in the last column of Table 4. The calculated secular change in PMC albedo from the multiple regression fit substantially exceeds the 95% confidence level for all latitude bands.

[36] The PMC albedo is observed to increase with latitude and to be higher in the Northern Hemisphere than the Southern Hemisphere, consistent with the observations from SME [*Thomas and Olivero*, 1989] and from SNOE [*Bailey et al.*, 2005]. This increase with latitude is also what would be expected given the increase of PMC particle size with latitude reported by *Karlsson and Rapp* [2006]. In order to understand the latitude dependence of our fit results, the 50°–64° latitude band discussed in this paper can be thought of as the "NLC zone," where visible observations of noctilucent clouds are possible. In this zone, relatively warm summer mesopause temperatures can make PMC formation marginal, particularly the bright clouds observed by SBUV instruments. The 64°–74° and 74°–82° latitude bands can be considered as the "PMC zone," where lower mesopause temperatures are consistently sufficient for ice formation. We find no significant difference between latitude bands within this zone. Note that, in both hemispheres, long-term albedo trends in the PMC zone are stronger than trends in the NLC zone at the edge of the cloud occurrence region. This remarkable result is counterintuitive to our current understanding of why PMCs should be brightening over time, namely, that the warmer regions closer to the equator, being nearer the frost point, would exhibit a greater response to a lowering of temperature and/or an increase in water vapor than regions at higher latitudes. The two-dimensional modeling results of the work by *Siskind et al.* [2005] support this concept, with substantial increases in the solar cycle response of both PMC brightness and equivalent ice content from high latitudes to lower latitudes. Our results imply that the brightest PMCs are most sensitive to external forcing influences, consistent with previous results based on *g*-distribution variations [*Thomas*, 2003], lidar data at ALOMAR [*Fiedler et al.*, 2005], and SAGE II PMC observations [*Shettle et al.*, 2002b].

[37] We caution again that the actual numerical values of the trends in Table 4 depend somewhat on our implemen-

tation of the ''consensus'' approach for combining multiple data sets. Other approaches, such as the ''backbone'' technique described by *Christy and Norris* [2004], are likely to yield different trend values. As a demonstration of this aspect, we created a combined SBUV PMC data set using the simplistic method of averaging all available albedo values within each season, without regard to possible instrument offsets. Multiple linear regression fits with Lyman alpha data again gave positive trend results, and all but one latitude band produced a larger long-term change than the values listed in Table 4. This particular approach (which we do not recommend) yields a strong latitude dependence in the SH results, with a +37% albedo increase over the SBUV data record at 50°–64°S decreasing to +12% at 74°–82°S. We cite these results as an illustration of the robustness of the qualitative long-term PMC behavior observed by SBUV instruments.

[38] The positive time lag between minimum solar activity and the PMC albedo maximum (listed in Table 4) continues to be a robust result of our analysis, consistent with the previous work, but remains a puzzle in terms of a physical mechanism. *Hervig and Siskind* [2006] reported a similar phase lag in the HALOE water vapor and PMC extinction data, but with no phase lag in concurrent mesospheric temperatures, suggesting that the phase lag in PMC brightness is linked to water vapor.

[39] The physical mechanisms responsible for the observed long-term variations in PMC albedo are not fully understood. *DeLand et al.* [2006] reviewed studies of mesospheric data and found that secular changes in water vapor seemed more likely than temperature changes. This result is consistent with recent microphysical modeling results by *Rapp and Thomas* [2006]. Recent three-dimensional model work by *von Zahn et al.* [2004] indicates that the solar cycle variation of H_2O at approximately 80 km for summer polar conditions may be significantly less than previously suggested [e.g., *Garcia*, 1989]. This former result is due to the inclusion of the ''freeze-drying'' effect, wherein ice particles form at ~85 km and sequester water vapor then descend to 80 km and sublime, releasing additional H_2O at altitudes where photolysis is weaker. However, PMC formation and brightness are so sensitive to changes in mesospheric temperature that a solar cycle variation of only a few degrees is also significant. *Hervig and Siskind* [2006] found a solar cycle variation of 4–5 K at 65°–70° and 80 km in UARS HALOE data. In contrast, *Lübken* [2000] found no significant solar cycle variation in falling sphere temperature data covering almost 40 years, although most of these data were collected near solar minimum periods. Dynamical effects such as planetary waves clearly affect PMC frequency and brightness on short timescales [e.g., *Kirkwood et al.*, 2002; *Merkel et al.*, 2003]. *Kirkwood and Stebel* [2003] found correlations between solar cycle variations in NLCs observed from northwestern Europe and planetary wave characteristics, but no convincing evidence for a long-term trend. Finally, it has been recently reported that tidal amplitudes at Halley Bay, Antarctica indicated a solar cycle variation and a positive secular trend [*Baumgaertner et al.*, 2005]. Some possible effects of such changes on PMC albedo, and thus on SBUV albedo trends, have been discussed by *Thomas et al.* [2006].

8. Conclusion

[40] The comprehensive temporal and geographic coverage of SBUV PMC data allows us to analyze long-term albedo variations as a function of latitude. The results presented in this paper use a revised PMC detection algorithm that has a more equal treatment of measurements at all local times and represent version 3 of the SBUV PMC data set. We have also developed an adjustment for the local time variations in PMC albedo that improves the agreement between measurements from concurrent SBUV instruments, leading to improved accuracy in the long-term fit results. We find that, when we construct composite data sets by combining data from all SBUV instruments, Northern Hemisphere PMC albedo values are larger than Southern Hemisphere albedo values in all latitude bands, which is in agreement with other measurements. We use a multiple linear regression fit to find an anticorrelation of PMC albedo with solar activity and an increasing long-term trend for all latitude bands in both Northern and Southern Hemispheres, consistent with the hemispherical average results obtained by *DeLand et al.* [2003]. Positive long-term trends are present regardless of the method used to create the composite albedo values. Response coefficients for 64°–74° and 74°–82° latitude are similar in magnitude, while fit coefficients for 50°–64° are smaller. The PMC response to solar activity is stronger in the Northern Hemisphere. The derived secular trends in PMC albedo now show no clear hemispheric difference, in contrast to our previous report [*Thomas et al.*, 2003]. We attribute this change in part to the use of a more rigorous method for treating interinstrument differences. More work is needed to understand the relative importance of mesospheric water vapor, temperature, and dynamical variations in influencing the long-term variability of PMC brightness. In particular, coincident measurements of PMC intensity, water vapor, and temperature such as those made by the UARS HALOE instrument [*Hervig and Siskind*, 2006] are crucial to determining PMC evolution. The Atmospheric Chemistry Experiment Fourier Transform Spectrometer instrument currently collects these measurements simultaneously [*Eremenko et al.*, 2005], and the Aeronomy of Ice in the Mesosphere (AIM) satellite will make common volume measurements of these quantities on every orbit.

[41] **Acknowledgments.** We thank the reviewers for useful comments that led to clarification of many portions of this paper. Michael Stevens provided valuable recommendations for the revisions to the PMC detection algorithm. Dave Rusch and Aimee Merkel provided helpful comments on the manuscript. The SBUV/2 data were obtained from NOAA/NESDIS with support from the NOAA Climate and Global Change Atmospheric Chemistry Element. Most of this work was supported by grants NAG5-13126 and NNX06AC96G from NASA's Office of Space Science.

References

Bailey, S. M., A. W. Merkel, G. E. Thomas, and J. N. Carstens (2005), Observations of polar mesospheric clouds by the Student Nitric Oxide Explorer, *J. Geophys. Res.*, *110*, D13203, doi:10.1029/2004JD005422.

Baumgaertner, A. J. M., A. J. McDonald, G. J. Fraser, and G. E. Plank (2005), Long-term observations of mean winds and tides in the upper mesosphere and lower thermosphere above Scott Base, Antarctica, *J. Atmos. Sol.-Terr. Phys.*, *67*, 1480–1496.

Christy, J. R., and W. B. Norris (2004), What may we conclude about global temperature trends?, *Geophys. Res. Lett.*, *31*, L06211, doi:10.1029/2003GL019361.

Chu, X., C. S. Gardner, and G. Pappen (2001), Lidar observations of polar mesospheric clouds at the South Pole: Diurnal variations, *Geophys. Res. Lett.*, *26*, 1937–1940.

DeLand, M. T., R. P. Cebula, L.-K. Huang, S. L. Taylor, R. S. Stolarski, and R. D. McPeters (2001), Observations of "hysteresis" in backscattered ultraviolet ozone data, *Journal of Atmospheric and Oceanic Technology*, *18*, 914–924.

DeLand, M. T., E. P. Shettle, G. E. Thomas, and J. J. Olivero (2003), Solar backscattered ultraviolet (SBUV) observations of polar mesospheric clouds (PMCs) over two solar cycles, *J. Geophys. Res.*, *108*(D8), 8445, doi:10.1029/2002JD002398.

DeLand, M. T., L.-K. Huang, S. L. Taylor, C. A. McKay, R. P. Cebula, P. K. Bhartia, and R. D. McPeters (2004), Long-term SBUV and SBUV/2 instrument calibration for Version 8 ozone data, in *Proceedings of the XX Quadrennial Ozone Symposium*, edited by C. S. Zerefos, University of Athens, Kos, Greece, 1–8 June 2004.

DeLand, M., E. Shettle, and M. Stevens (2005), Local time effects on trends in SBUV PMC data, paper IAGA2005-A-01129, paper presented at the 10th Scientific Assembly of the Int. Assoc. Geomag. and Aeronomy, Toulouse, France, 18–28 July 2005.

DeLand, M. T., E. P. Shettle, G. E. Thomas, and J. J. Olivero (2006), A quarter-century of satellite PMC observations, *J. Atmos. Sol.-Terr. Phys.*, *68*, 9–29.

Donahue, T. M., B. Guenther, and J. E. Blamont (1972), Noctilucent clouds in daytime: Circumpolar particulate layers near the summer mesopause, *J. Atmos. Sci.*, *30*, 515–517.

Eremenko, M. N., S. V. Petelina, A. Y. Zasetsky, B. Karlsson, C. P. Rinsland, E. J. Llewellyn, and J. J. Sloan (2005), Shape and composition of PMC particles derived from satellite remote sensing measurements, *Geophys. Res. Lett.*, *32*, L16S06, doi:10.1029/2005GL023013.

Fiedler, J., G. Baumgarten, and G. von Cossart (2005), Mean diurnal variations of noctilucent clouds during 7 years of lidar observations at ALOMAR, *Ann. Geophys.*, *23*, 1175–1181.

Fogle, B. (1965), Noctilucent clouds over Punta Arena, Chile, *Nature*, *207*, 66.

Garcia, R. R. (1989), Dynamics, radiation, and photochemistry in the mesosphere: Implications for the formation of noctilucent clouds, *J. Geophys. Res.*, *94*, 14,605–14,616.

Gleason, J. F., and R. D. McPeters (1995), Corrections to the Nimbus 7 solar backscatter ultraviolet data in the "nonsync" period (February 1987 to June 1990), *J. Geophys. Res.*, *100*, 16,873–16,877.

Hervig, M., and D. Siskind (2006), Decadal and inter-hemispheric variability in polar mesospheric clouds, water vapor, and temperature, *J. Atmos. Sol.-Terr. Phys.*, *68*, 30–41.

Hervig, M. E., R. E. Thompson, M. E. McHugh, L. L. Gordley, J. M. Russell III, and M. E. Summers (2001), First confirmation that water ice is the primary component of polar mesospheric clouds, *Geophys. Res. Lett.*, *28*, 971–974.

Hilsenrath, E., R. P. Cebula, M. T. DeLand, K. Laamann, S. Taylor, C. Wellemeyer, and P. K. Bhartia (1995), Calibration of the NOAA-11 solar backscatter ultraviolet (SBUV/2) ozone data set from 1989 to 1993 using in-flight calibration data and SSBUV, *J. Geophys. Res.*, *100*, 1351–1366.

Janz, S., E. Hilsenrath, J. Butler, D. F. Heath, and R. P. Cebula (1995), Uncertainties in radiance calibrations of backscatter ultraviolet (BUV) instruments, *Metrologia*, *32*, 637–641.

Karlsson, B., and M. Rapp (2006), Latitudinal dependence of noctilucent cloud growth, *Geophys. Res. Lett.*, *33*, L11812, doi:10.1029/2006GL025805.

Kirkwood, S., and K. Stebel (2003), Influence of planetary waves on noctilucent cloud occurrence over NW Europe, *J. Geophys. Res.*, *108*(D8), 8440, doi:10.1029/2002JD002356.

Kirkwood, S., V. Barabash, B. U. E. Brändström, A. Moström, K. Stebel, N. Mitchell, and W. Hocking (2002), Noctilucent clouds, PMSE, and 5-day planetary waves: A case study, *Geophys. Res. Lett.*, *29*(10), 1411, doi:10.1029/2001GL014022.

Lübken, F.-J. (2000), Nearly zero temperature trend in the polar summer mesosphere, *Geophys. Res. Lett.*, *27*, 3603–3606.

Merkel, A. W., G. E. Thomas, S. E. Palo, and S. M. Bailey (2003), Observations of the 5-day planetary wave in PMC measurements from the Student Nitric Oxide Explorer Satellite, *Geophys. Res. Lett.*, *30*(4), 1196, doi:10.1029/2002GL016524.

Rapp, M., and G. E. Thomas (2006), Modeling the microphysics of mesospheric ice particles—Assessment of current capabilities and basic sensitivities, *J. Atmos. Sol.-Terr. Phys.*, *68*, 715–744.

Shettle, E. P., G. E. Thomas, J. J. Olivero, W. F. J. Evans, D. J. Debrestian, and L. Chardon (2002a), Three satellite comparison of polar mesospheric clouds: Evidence for long-term change, *J. Geophys. Res.*, *107*(D12), 4134, doi:10.1029/2001JD000668.

Shettle, E. P., S. P. Burton, J. J. Olivero, G. E. Thomas, and L. W. Thomason (2002b), SAGE II measurements of polar mesospheric clouds, *Memoirs Brit. Astron. Assoc.*, 45, papers given at the Perth meeting on mesospheric clouds, edited by M. Gadsden and N. James.

Shettle, E. P., M. T. DeLand, G. E. Thomas, and J. J. Olivero (2005), Multi-decadal variations in the brightness of polar mesospheric clouds, *Eos Trans. AGU*, *86*(18), Jt. Assem. Suppl., Abstract SA51A-02.

Siskind, D. E., M. H. Stevens, and C. R. Englert (2005), A model study of global variability in mesospheric cloudiness, *J. Atmos. Sol.-Terr. Phys.*, *67*, 501–513.

Stevens, M. H., J. Gumbel, C. R. Englert, K. U. Grossmann, M. Rapp, and P. Hartogh (2003), Polar mesospheric clouds formed from space shuttle exhaust, *Geophys. Res. Lett.*, *30*(10), 1546, doi:10.1029/2003GL017249.

Stevens, M. H., C. R. Englert, and M. T. DeLand (2004), What anthropogenic changes are reflected in the mesospheric cloud record?, paper C2.5-0001-04 presented at the 35th COSPAR Scientific Assembly, Paris, 18–25 July 2004.

Taylor, S. L., R. P. Cebula, M. T. DeLand, L.-K. Huang, R. S. Stolarski, and R. D. McPeters (2003), Improved calibration of NOAA-9 and NOAA-11 SBUV/2 total ozone data using in-flight validation methods, *Int. J. Remote Sens.*, *24*, 315–328.

Thayer, J. P., M. Rapp, A. J. Gerrard, E. Gudmundsson, and T. J. Kane (2003), Gravity wave influences on Arctic mesospheric clouds as determined by a Rayleigh lidar at Sondrestrom, Greenland, *J. Geophys. Res.*, *108*(D8), 8449, doi:10.1029/2002JD002363.

Thomas, G. E. (1996), Global change in the mesosphere-lower thermosphere region: Has it already arrived?, *J. Atmos. Sol.-Terr. Phys.*, *58*, 1629–1656.

Thomas, G. E. (2003), Are noctilucent clouds harbingers of global change in the middle atmosphere?, *Adv. Space Res.*, *32*, 1737–1746.

Thomas, G. E., and J. J. Olivero (1989), Climatology of polar mesospheric clouds: 2. Further analysis of Solar Mesospheric Explorer data, *J. Geophys. Res.*, *94*, 14,673–14,702.

Thomas, G. E., and J. J. Olivero (2001), Noctilucent clouds as possible indicators of global change in the mesosphere, *Adv. Space Res.*, *28*, 937–946.

Thomas, G. E., J. J. Olivero, E. J. Jensen, W. Schröder, and O. B. Toon (1989), Relation between increasing methane and the presence of ice clouds at the mesopause, *Nature*, *338*, 490–492.

Thomas, G. E., J. J. Olivero, M. DeLand, and E. P. Shettle (2003), Comment on "Are noctilucent clouds truly a 'miner's canary' for global change?", *Eos Trans. AGU*, *84*, 352–353.

Thomas, G. E., M. Rapp, S. Palo, M. DeLand, and A. Baumgaertner (2006), Long-term variations of PMC brightness and occurrence frequency: Are they caused by changes in atmospheric tides?, *Eos Trans. AGU*, *87*(36), Jt. Assem. Suppl., Abstract SA51A-01.

von Zahn, U., U. Berger, J. Fiedler, and P. Hartogh (2004), Noctilucent clouds and mesospheric water vapor: The past decade, *Atmos. Chem. Phys.*, *4*, 2449–2464, www.atmos-chem-phys.org/acp/4/2449, Sref-ID: 1680-7324/acp/2004-4-2449.

Weatherhead, E. C., et al. (1998), Factors affecting the detection of trends: Statistical considerations and applications to environmental data, *J. Geophys. Res.*, *103*, 17,149–17,161.

Woods, T. N., et al. (1996), Validation of the UARS solar ultraviolet irradiances: Comparisons with the ATLAS 1 and 2 measurements, *J. Geophys. Res.*, *101*, 9541–9569.

Woods, T. N., W. K. Tobiska, G. J. Rottman, and J. R. Worden (2000), Improved solar Lyman α irradiance modeling from 1947 through 1999 based on UARS observations, *J. Geophys. Res.*, *105*, 27,195–27,215.

Woods, T. N., F. G. Eparvier, S. M. Bailey, P. C. Chamberlin, J. Lean, G. J. Rottman, S. C. Solomon, W. K. Tobiska, and D. L. Woodraska (2005), The Solar EUV Experiment (SEE): Mission overview and first results, *J. Geophys. Res.*, *110*, A01312, doi:10.1029/2004JA010765.

M. T. DeLand, Science Systems and Applications, Inc. (SSAI), 10210 Greenbelt Road, Suite 600, Lanham, MD 20706, USA. (matthew_deland@ssaihq.com)

J. J. Olivero, Department of Physical Sciences, Embry-Riddle Aeronautical University, Daytona Beach, FL 32114, USA.

E. P. Shettle, Remote Sensing Division, Naval Research Laboratory, Code 7227, Washington, DC 20375-5351, USA.

G. E. Thomas, Laboratory for Atmospheric and Space Physics, University of Colorado, Boulder, CO 80309-0392, USA.